Heliyon 7 (2021) e06527

Contents lists available at ScienceDirect

Heliyon

journal homepage: www.cell.com/heliyon

Research article

# Growth, spectral, optical, electrical and computational analysis of sodium oxalate single crystals

R. Ramalakshmi [a], S. Stella Mary [a,**], S. Shahil Kirupavathy [b], S. Muthu [c,*], Renjith Thomas [d]

[a] Department of Physics, St.Peter's Institute of Higher Education and Research, Avadi, Chennai, 600 054, India
[b] Department of Physics, Velammal Engineering College, Chennai, 600 066, India
[c] Department of Physics, Arignar Anna Govt. Arts College, Cheyyar, 604 407, Tamil Nadu, India
[d] Department of Chemistry, St Berchmans College (Autonomous), Changanassery, 686101, Kerala, India

ARTICLE INFO

*Keywords:*
DFT
FTIR
Growth from solution
NLO

ABSTRACT

Single crystals of Sodium Oxalate (SO) were grown by adopting the slow evaporation solution growth approach from aqueous solution. The prominent functional groups seen in the SO crystal were distinctly detected with Fourier transform infrared and FT-Raman spectral analysis. The cut-off wavelength of 230 nm was measured using Ultraviolet -visible spectral analysis. Theoretical quantum chemical computations were done by DFT using Gaussian software package. The different properties such as structural, vibrational and electronic properties of SO was studied at the B3LYP/LanL2DZ level. The chemical activity of SO molecule was revealed by HOMO-LUMO energies. From Topology analysis the chemical significance of the molecules has been enunciated. The electron density centered on local reactivity descriptors like Mulliken atomic charges and Fukui function were calculated to describe the chemical reactivity of the SO compound. The mechanical property of the grown crystal was disclosed from Vicker's micro hardness test carried out on the grown SO crystals and the test confirms the soft nature of the crystal. The dielectric behavior of SO crystal was completely investigated for different temperatures and the activation energies were calculated for different frequencies.

## 1. Introduction

Organic nonlinear optical crystals are mostly attracting all researchers owing to their diversity in potential area of applications like photonics, doubling of frequency, optical switching, modulation, laser remote sensing and optical device fabrication. Also, there is a demand for growing crystals with increased nonlinear optical behaviour as it has great demand for applications in the field of electronics, optical communication and storage systems [1].

The high degree of delocalized π electrons in organic materials are responsible for their nonlinear response [2]. Significant NLO responses are exhibited by organic compounds owing to the availability of donor and acceptor network in their molecular structure which in turn enable them to offer enormous design possibilities. Furthermore, organic materials stay advantageous as the synthetic flexibility found in them enable to customize the optical properties by enhancing structural reformation and unveil massive laser damage threshold.

The ferroelectric behavior of numerous oxalate compounds has extensive usages in electronic and acoustic optical devices [3, 4, 5]. Among the various acids available, oxalic acid stays as a strong acid [6] due to the presence of directly attached two carboxyl groups. Human body generates oxalic acid naturally during metabolization of ascorbic acid and glycine. It has been reported that a number of oxalates like barium oxalate [7], barium ammonium oxalate [8], cadmium oxalate [9], cobalt oxalate [10], sodium oxalate [11] etc., are grown using gel technique. Among the various salts of oxalic acid, it is noted that though sodium oxalate is highly toxic, it is used in industries for metal cleaning, leather tanning, electroplating wash, etc. Sodium Oxalate (SO) is an innocuous compound which is found in the Kamias fruit and this compound possesses significant chemical properties which prove to be effective in the destruction of Chlorofluorocarbons.

Literature survey revealed that SO crystals were grown by Gel Growth [11]. Significant applications exhibited by SO motivated to grow sodium oxalate crystals by slow evaporation solution growth technique and analyze its spectral, optical, mechanical and dielectric characteristics

* Corresponding author.
** Corresponding author.
*E-mail addresses:* celstel1968@gmail.com (S. Stella Mary), mutgee@gmail.com (S. Muthu).

https://doi.org/10.1016/j.heliyon.2021.e06527
Received 16 September 2020; Received in revised form 10 December 2020; Accepted 11 March 2021

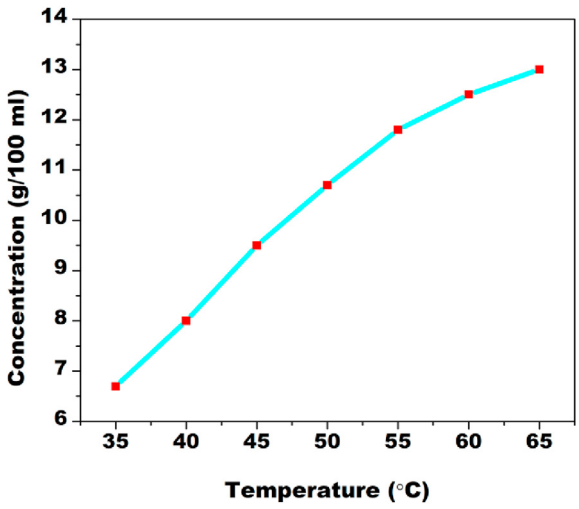


**Figure 1.** Solubility curve of SO.

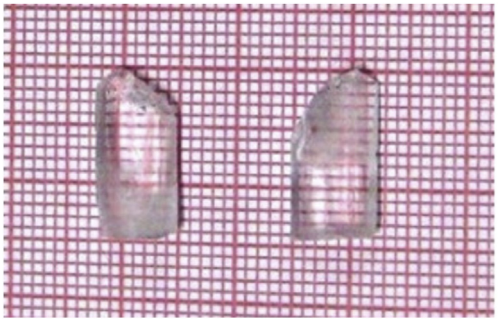

**Figure 2.** As grown SO crystals.

**Table 1.** Atomic coordinates of SO.

| Atomic co-ordinates in fractions of monoclinic axes | | | |
|---|---|---|---|
| | x | y | Z |
| Na | 0.3020 (3) | 0.0565 (2) | 0.3552 (1) |
| O1 | 0.1657 (5) | -0.1222 (4) | 0.1511 (1) |
| O2 | 0.2274 (6) | 0.2704 (3) | 0.0691 (2) |
| C | 0.1135 (8) | 0.0435 (4) | 0.0634 (3) |

Atomic co-ordinates taken from Ref. [21].

using various instrumentation approaches. Several researchers have done extensive theoretical studies on oxalate crystals [12, 13, 14]. This encouraged us to carry out theoretical studies like HOMO-LUMO, NBO, MEPs, Topology and Fukui characteristics for SO. All the obtained results are elaborately presented in this paper.

## 2. Experimental approaches

### 2.1. Growth of sodium oxalate crystals

Sodium oxalate (SO) crystals were grown from the commercially available sodium oxalate (98% pure form) purchased from Merck Company. To obtain crystals of good quality, the obtained SO crystals were refined by adopting the repeated recrystallization process using deionized water as solvent. The solution was stirred continuously and the saturated level of SO was obtained at 45 °C. Solubility test unveil water as a good solvent to grow SO. The solubility curve for SO in water presented in Figure 1 shows a positive gradient of solubility.

The beaker containing saturated SO solution with a seed crystal free of inclusions was placed in a constant temperature bath held at 37 °C for slow evaporation of solvent. Transparent SO crystals were harvested after 50 days. Figure 2 shows the as grown crystals of SO.

### 2.2. Characterizations

Many characterization techniques such as FTIR and FT-Raman analysis, UV–Visible spectral analysis, micro hardness and dielectric have been applied to the grown SO crystals. The optical UV–Vis spectrum was investigated by the LAMBDA-35 UV–Vis spectrophotometer. FTIR and FT-Raman studies was done using FT-IR ATR spectrophotometer and BRUKER: RFS 27 spectrometer respectively and from the obtained results the diverse vibrational modes of SO were identified. Leitz wetzler Vickers microhardness tester performed microhardness analysis and brought into light the mechanical stability. Dielectric studies using HP 4275 LCR meter at different temperatures were carried out.

### 2.3. Computational details

The quantum chemical calculations of SO was done using the Becke 3-Lee-Yang-parr (B3LYP)/LanL2DZ level of theory employed in the Gaussian 09W program package [15]. To begin with, the atomic co-ordinates for optimizing the molecular geometry was envisioned using the Gauss View 5.0 software package [16]. Molecular structure of SO was augmented by DFT at the B3LYP/6-311++G (d,p) level of theory, and the obtained structure was further adopted for calculating the frequency of vibration. In addition, the measured frequencies of vibration were assigned after analyzing every fundamental modes of vibration using the VEDA 4 program [17, 18] utilizing the potential energy distribution (PED). The theoretical molecular interactions were calculated from HOMO-LUMO analysis to study the electronic properties. The stabilization energies were calculated from NBO analysis. Electron localization function (ELF) and localized orbital locator (LOL) figures supported to compute the distribution of electrons and also their reactive sites on the

**Table 2.** Geometrical parameters of optimized SO; bond length (Å) and bond angle (o) with B3LYP/LanL2DZ basis set.

| Parameters | Bond length ($A^0$) | | Parameters | Bond Angle ($^0$) | |
|---|---|---|---|---|---|
| Atom | Experimental[a] | B3LYP/LanL2DZ | Atom | Experimental[a] | B3LYP/LanL2DZ |
| C1–O2 | 1.265 | 1.301 | O3–C1–O2 | 125.8 | 122.92 |
| C1–O3 | 1.253 | 1.301 | O2–C1–C4 | 117.3 | 118.54 |
| C1–C4 | 1.568 | 1.527 | O5–C4–O6 | 125.8 | 122.91 |
| C4–O5 | 1.253 | 1.302 | C1–O5–C4 | 116.9 | 118.54 |
| C4–O6 | 1.265 | 1.301 | O6–C4–C1 | 117.3 | 118.55 |
| | | | O3–C1–C4 | 116.9 | 118.53 |

**Experimental[a] taken from Ref.** [21].
RMSD for bond length 0.04237(Å).
RMSD for bond Angle 2.045(Å).

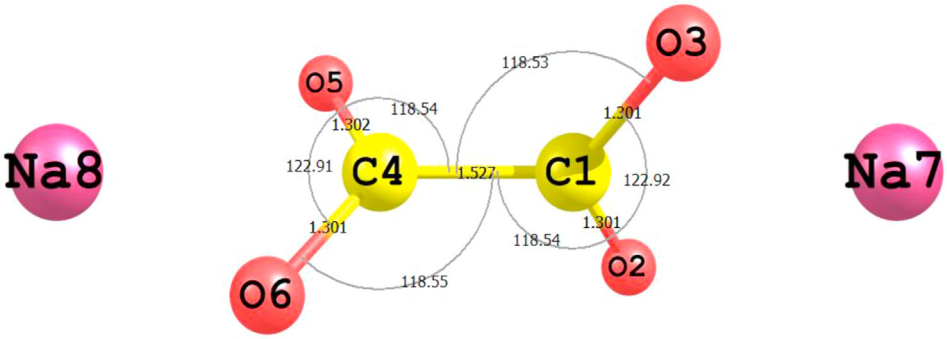


**Figure 3.** Optimized geometric structure of SO with atoms numbering.

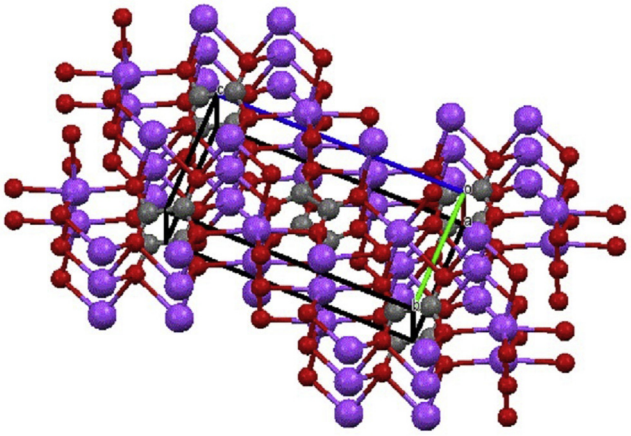

**Figure 4.** Crystal packing of SO.

title compound. Descriptors of local reactivity like electrophilic, nucleophilic and local softness were calculated from Mulliken atomic charges [19] of SO using DFT method with 6–311++G (d, p) basis set.

## 3. Results and discussion

### 3.1. Molecular geometry

Experimental studies carried out on SO crystals by Jeffrey and Parry brought into light that SO crystallizes in the centrosymmetric crystal system with space group $P2_1/a$ [20]. Further refinement on the structure of SO by D.A. Reed and M.M. Olmstead reports that SO possess the monoclinic crystal system with space group $P2_1/c$ and lattice parameters as a = 3.449 (2) Å, b = 5.243 (3) Å, c = 10.375 (4) Å, β = 92.66 (4)°. The bond lengths exhibited are given in Table 1 [21]. The bond parameters (bond length and bond angles) of SO molecule were computed using the

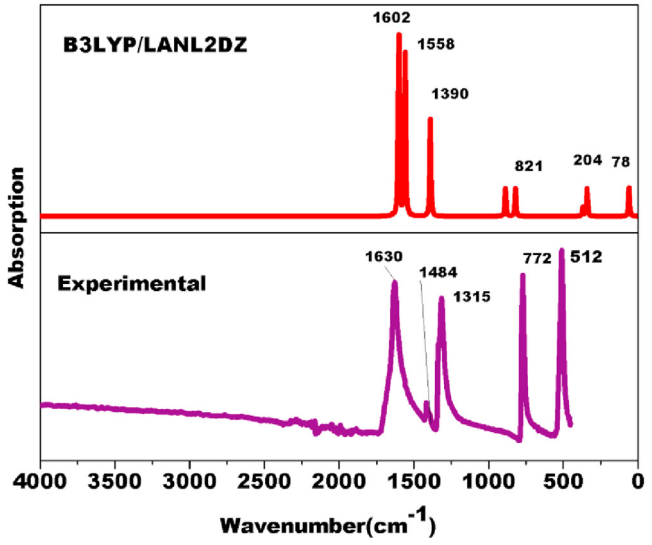


**Figure 5.** Experimental and theoretical FT-IR spectra of title compound by the DFT/B3LYP/LanL2DZ basis set.

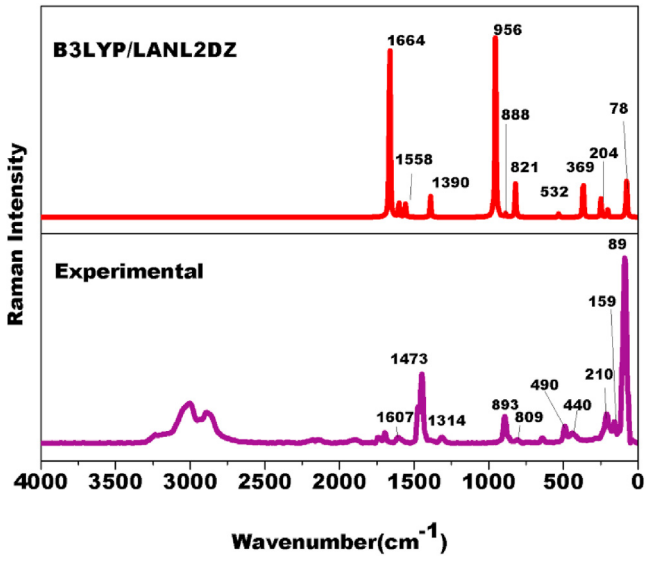


**Figure 6.** Experimental and theoretical FT Raman spectra of title compound by the DFT/B3LYP/LanL2DZ basis set.

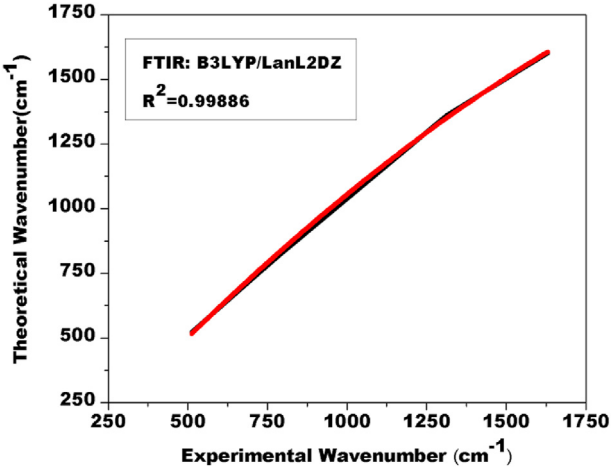


**Figure 7.** Correlation graph of Experimental and theoretical FTIR spectra of title compound by the DFT/B3LYP/LanL2DZ basis set.

**Table 3.** Experimental and theoretical vibrational frequency (unscaled and scaled) assignment with (PED%) of SO compound using B3LYP/LanL2DZ.

| Mode no. | Experimental wavenumber ($cm^{-1}$) | | Theoritical wavenumber ($cm^{-1}$) | | | | | | Assignments |
|---|---|---|---|---|---|---|---|---|---|
| | FTIR | FTRaman | Un scaled | scaled | IR Intensity | | Raman Intensity | | |
| | | | | | Relative | Absolute[a] | Relative | Absolute[b] | (PED %) |
| 18 | | | 1664 | 1664 | 0 | 0 | 19 | 95 | γOC(50)+ γCC(35) |
| 17 | 1630 | 1606 | 1602 | 1602 | 805 | 100 | 1 | 7 | γOC(94) |
| 16 | | | 1558 | 1558 | 740 | 92 | 1 | 6 | γOC(92) |
| 15 | 1315 | 1314 | 1390 | 1362 | 434 | 54 | 2 | 11 | γOC(88) |
| 14 | | | 956 | 937 | 0 | 0 | 20 | 100 | γOC(44)+ γCC(24)+ βOCO(30) |
| 13 | | 893 | 888 | 870 | 68 | 8 | 0 | 1 | βOCC(10)+ βCCO(10)+ ωOCOC(36)+ ωCOOC(33) |
| 12 | | | 888 | 870 | 68 | 8 | 0 | 1 | βOCC(10)+ βCCO(10)+ ωOCOC(36)+ ωCOOC(33) |
| 11 | 772 | 809 | 821 | 805 | 126 | 16 | 3 | 15 | βOCO(88) |
| 10 | 512 | 490 | 532 | 522 | 0 | 0 | 0 | 2 | γCC(27)+ γNaO(20)+ βOCO(48) |
| 9 | | 440 | 369 | 361 | 23 | 3 | 2 | 8 | βNaOC(26)+ βOCC(22)+ βCCO(22) |
| 8 | | | 369 | 361 | 23 | 3 | 2 | 8 | βNaOC(26)+ βOCC(22)+ βCCO(22) |
| 7 | | | 341 | 334 | 129 | 16 | 0 | 0 | γNaO(74)+ βNaOC(24) |
| 6 | | 210 | 249 | 212 | 0 | 0 | 2 | 8 | γCC(14)+ γNaO(46)+ βNaOC(28) |
| 5 | | 159 | 204 | 173 | 0 | 0 | 0 | 2 | βNaOC(42)+βOCC(13)+ βCCO(13) |
| 4 | | | 204 | 173 | 0 | 0 | 0 | 2 | βNaOC(42)+ βOCC(13)+ βCCO(13) |
| 3 | | 89 | 78 | 66 | 0 | 0 | 3 | 16 | τOCCO(100) |
| 2 | | | 62 | 53 | 67 | 8 | 0 | 0 | τOCONa(33)+ τNaOCC(42)+ ωCOOC(10) |
| 1 | | | 62 | 53 | 67 | 8 | 0 | 0 | τOCONa(33)+ τNaOCC(42)+ ωCOOC(10) |

γ-stretching, β-bending,τ-torsion, ω-out of plan bending.
[a] Relative absorption intensity normalized with 100 for topmost peak absorption.
[b] Relative Raman intensities normalized to 100.

**Table 4.** Calculated energy values of SO.

| Basic set | B3LYP/6-311++G (d,p) |
|---|---|
| $E_{HOMO}$ (eV) | -5.6211 |
| $E_{LUMO}$ (eV) | -0.9233 |
| Ionization potential (IP) | 5.6211 |
| Electron affinity (EA) | 0.9233 |
| Energy gap (eV) | 4.6978 |
| Electronegativity (χ) | 3.2722 |
| Chemical potential (μ) | -3.2722 |
| Chemical hardness (η) | 2.3489 |
| Chemical softness (S) | 0.2129 |
| Electrophilicity index (ω) | 2.2792 |

DFT/B3LYP method with 6–311++G (d,p) basis set by considering the crystallography data reported by D.A. Reed. Table 2 presents comparison of experimental [21] and theoretically calculated bond length and bond angle values. The optimized molecular structure of SO is given in Figure 3 and the crystal packing is shown in Figure 4. From theoretical calculations it is predicted that the homonuclear bond C1–C4 have higher bond length of 1.527 Å while the experimental value was found to be 1.568 Å. The heteronuclear bonds (C1–O2, C1–O3, C4–O5, C4–O6) have lesser bond lengths of 1.265 Å, 1.253 Å, 1.253 Å and 1.265 Å experimentally and 1.301 Å, 1.301 Å, 1.302 Å and 1.301 Å from theoretical study. The observed longer lengths of homonuclear bond when compared to the heteronuclear bonds is due to the repulsive nature of like charges and attractive character of unlike charges. The bond angle O3–C1–O2 and O5–C4–O6 are larger than the other bond angle calculated by both experimental and theoretical. This variation in bond angle is because the repulsive forces reduce the distance between the two oxygen atoms. The force of repulsion ensuing between two oxygen led to an increase in the angle owing to the shorter distance between the two oxygen and thereby reduce the repulsion.

### 3.2. FT-IR and FT-Raman vibrational analysis

FT-IR studies provide enumerative and qualitative evaluation for organic and inorganic samples and stay as an important analytical method for identifying different functional groups and learn information on the covalent bonding. This investigation produces an infrared absorption spectrum and help to pinpoint the various chemical bonds available in a molecule. The spectra give the profile of the sample through a unique molecular finger print which can screen and scan samples for various components.

SO compound consist of eight atoms with eighteen normal modes of vibration. The spectrum obtained through theoretical computation at the B3LYP/Lan2DZ level of theory is shown in Figures 5 and 6 in comparison with the experimental spectrum. Here, the obtained Raman activities are

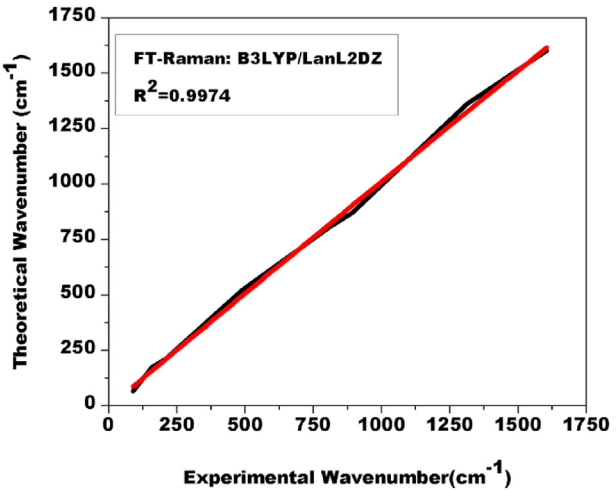


**Figure 8.** Correlation graph of Experimental and theoretical FT Raman spectra of title compound by the DFT/B3LYP/LanL2DZ basis set.

**Table 5.** Second order perturbation theory of the Fock matrix NBO analysis of SO.

| DonorNBO(i) | Type | ED/e | AcceptorNBO(j) | Type | ED/e | $E^{(2)}$[a] | E(j)-E(i)[b] | F (i,j)[c] |
|---|---|---|---|---|---|---|---|---|
| | | | | | | kcal/mola.u. | a.u. | a.u. |
| O3–C4 | σ | 1.97936 | C5 | | 0.00009 | 0.82 | 2.2 | 0.038 |
| O3–C4 | σ | 1.97936 | C4–O8 | σ* | 0.00005 | 0.97 | 1.62 | 0.036 |
| O3–C4 | σ | 1.97936 | C5–O7 | σ* | 0.00796 | 0.85 | 1.44 | 0.032 |
| O3–H9 | σ | 1.98048 | C4 | | | 1.69 | 2.1 | 0.053 |
| O3–H9 | σ | 1.98048 | C4 | | 0.01155 | 3 | 2.66 | 0.08 |
| O3–H9 | σ | 1.98048 | C4–C5 | σ* | 0.00008 | 0.91 | 1.1 | 0.029 |
| O3–H9 | σ | 1.98048 | C4–O8 | σ* | 0.00005 | 6.12 | 1.38 | 0.082 |
| C4–C5 | σ | 1.98843 | O3 | | 0.00001 | 0.68 | 1.41 | 0.028 |
| C4–C5 | σ | 1.98843 | O6 | | 0.00001 | 1.25 | 1.38 | 0.037 |
| C4–C5 | σ | 1.98843 | O7 | | 0.00001 | 0.6 | 1.39 | 0.026 |
| C4–C5 | σ | 1.98843 | O8 | | | 1.14 | 1.43 | 0.036 |
| C4–C5 | σ | 1.98843 | C4–O8 | σ* | 0.00005 | 0.63 | 1.29 | 0.025 |
| C4–C5 | σ | 1.98843 | O7–H10 | σ* | 0.00319 | 3.24 | 1.04 | 0.052 |
| C4–O8 | σ | 1.98856 | C4 | | | 1.12 | 2.23 | 0.045 |
| C4–O8 | σ | 1.98856 | O3–C4 | σ* | 0.00018 | 1.38 | 1.49 | 0.041 |
| C4–O8 | σ | 1.98856 | O3–H9 | σ* | 0.00009 | 1.15 | 1.44 | 0.036 |
| C4–O8 | σ | 1.98856 | C5–O6 | σ* | 0.00002 | 0.6 | 1.62 | 0.028 |
| C4–O8 | π | 1.97867 | O3 | | 0.00001 | 0.85 | 0.98 | 0.026 |
| C4–O8 | π | 1.97867 | C4–O8 | π* | 0.00005 | 0.64 | 0.38 | 0.015 |
| C4–O8 | π | 1.97867 | C5–O6 | π* | 0.00001 | 6.65 | 0.36 | 0.046 |
| C5–O6 | σ | 1.96618 | C5 | | 0.00009 | 1.14 | 2.25 | 0.045 |
| C5–O6 | σ | 1.96618 | C4–O8 | σ* | 0.00005 | 0.74 | 1.68 | 0.032 |
| C5–O6 | σ | 1.96618 | C5–O7 | σ* | 0.00796 | 0.73 | 1.49 | 0.03 |
| C5–O6 | π | 1.96076 | O7 | | 0.00001 | 0.84 | 0.95 | 0.025 |
| C5–O6 | π | 1.96076 | C4–O8 | π* | 0.00005 | 5.4 | 0.4 | 0.044 |
| C5–O6 | π | 1.96076 | C5–O6 | π* | 0.00001 | 0.8 | 0.38 | 0.017 |
| C5–O7 | σ | 1.97002 | C4 | | | 0.94 | 2.22 | 0.041 |
| C5–O7 | σ | 1.97002 | H10 | | 0.00079 | 0.55 | 2.53 | 0.033 |
| C5–O7 | σ | 1.97002 | O3–C4 | σ* | 0.00018 | 0.65 | 1.48 | 0.028 |
| C5–O7 | σ | 1.97002 | C5–O6 | σ* | 0.00002 | 1.04 | 1.61 | 0.037 |
| O7–H10 | σ | 1.98594 | C5 | | 0.00009 | 1.78 | 1.96 | 0.053 |
| O7–H10 | σ | 1.98594 | C5 | | 0.00003 | 0.86 | 1.93 | 0.036 |
| O7–H10 | σ | 1.98594 | C5 | | 0.00268 | 0.88 | 2.77 | 0.044 |
| O7–H10 | σ | 1.98594 | C4–C5 | σ* | 0.00008 | 4.4 | 1.12 | 0.064 |
| O7–H10 | σ | 1.98594 | C5–O6 | σ* | 0.00002 | 1.06 | 1.34 | 0.034 |
| O6 | CR (1) | 1.96947 | C5–O7 | σ* | 0.00796 | 0.7 | 19.3 | 0.105 |
| O7 | CR (1) | 1.64766 | C5 | | 0.00009 | 1.95 | 20.16 | 0.178 |
| O7 | CR (1) | 1.64766 | C5 | | 0.00003 | 1.1 | 20.13 | 0.133 |
| O7 | CR (1) | 1.64766 | C5 | | 0.00381 | 0.83 | 20.66 | 0.117 |
| O7 | CR (1) | 1.64766 | C5–O6 | σ* | 0.00002 | 0.63 | 19.54 | 0.1 |
| O8 | CR (1) | 1.97674 | C4 | | | 5.89 | 20.02 | 0.308 |
| | | | | | | | | |
| O8 | CR (1) | 1.97674 | O3–C4 | σ* | 0.00018 | 0.81 | 19.29 | 0.113 |
| O3 | LP (1) | 1.97772 | C4 | | | 3.08 | 1.93 | 0.069 |
| O3 | LP (1) | 1.97772 | C4 | | 0.01155 | 0.77 | 2.49 | 0.039 |
| O3 | LP (1) | 1.97772 | C4 | | 0.00489 | 1.4 | 2.92 | 0.057 |
| O3 | LP (1) | 1.97772 | H9 | | 0.00001 | 1.18 | 1.28 | 0.035 |
| O3 | LP (1) | 1.97772 | H9 | | 0.00829 | 0.88 | 2.03 | 0.038 |
| O3 | LP (1) | 1.97772 | C4–C5 | σ* | 0.00008 | 5.96 | 0.94 | 0.068 |
| O3 | LP (1) | 1.97772 | C4–O8 | σ* | 0.00005 | 1.25 | 1.21 | 0.035 |
| O3 | LP (2) | 1.97688 | C4 | | | 3.29 | 1.93 | 0.075 |
| O3 | LP (2) | 1.97688 | H9 | | | 1.17 | 1.72 | 0.042 |
| O3 | LP (2) | 1.97688 | H9 | | 0.00001 | 0.59 | 1.75 | 0.03 |
| O3 | LP (2) | 1.97688 | C4–O8 | π* | 0.00005 | 56.37 | 0.35 | 0.125 |
| O6 | LP (1) | 1.97714 | C5 | | 0.00009 | 13.65 | 1.92 | 0.144 |
| O6 | LP (1) | 1.97714 | C5 | | 0.00003 | 0.98 | 1.89 | 0.038 |
| O6 | LP (1) | 1.97714 | C5 | | 0.00381 | 0.71 | 2.42 | 0.037 |

(*continued on next page*)

**Table 5** (*continued*)

| DonorNBO(i) | Type | ED/e | AcceptorNBO(j) | Type | ED/e | E(2)[a] kcal/mola.u. | E(j)-E(i)[b] a.u. | F (i,j)[c] a.u. |
|---|---|---|---|---|---|---|---|---|
| O6 | LP (1) | 1.97714 | C5 | | 0.00268 | 0.56 | 2.73 | 0.035 |
| O6 | LP (1) | 1.97714 | C5 | | 0.00006 | 0.84 | 6.87 | 0.068 |
| O6 | LP (1) | 1.97714 | C4–C5 | σ* | 0.00008 | 1.15 | 1.07 | 0.032 |
| O6 | LP (1) | 1.97714 | C5–O7 | σ* | 0.00796 | 1.43 | 1.16 | 0.037 |
| O6 | LP (2) | 1.97923 | C5 | | 0.00003 | 3.09 | 1.45 | 0.062 |
| O6 | LP (2) | 1.97923 | C5 | | 0.00381 | 0.55 | 1.98 | 0.03 |
| O6 | LP (2) | 1.97923 | O3–H9 | σ* | 0.00009 | 2.21 | 0.68 | 0.036 |
| O6 | LP (2) | 1.97923 | C4–C5 | σ* | 0.00008 | 18 | 0.63 | 0.095 |
| O6 | LP (2) | 1.97923 | C4–O8 | σ* | 0.00005 | 0.6 | 0.9 | 0.021 |
| O6 | LP (2) | 1.97923 | C5–O7 | σ* | 0.00796 | 25.78 | 0.72 | 0.123 |
| O7 | LP (1) | 1.66776 | C5 | | 0.00009 | 3.98 | 1.81 | 0.076 |
| O7 | LP (1) | 1.66776 | C5 | | 0.00381 | 2.25 | 2.32 | 0.065 |
| O7 | LP (1) | 1.66776 | H10 | | 0.00165 | 1.22 | 2.52 | 0.05 |
| O7 | LP (1) | 1.66776 | C4–C5 | σ* | 0.00008 | 1.33 | 0.97 | 0.033 |
| O7 | LP (1) | 1.66776 | C5–O6 | σ* | 0.00002 | 9.12 | 1.19 | 0.093 |
| O7 | LP (2) | 1.98079 | C5 | | 0.00001 | 3.38 | 1.94 | 0.077 |
| O7 | LP (2) | 1.98079 | H10 | | 0.00154 | 1.68 | 1.84 | 0.053 |
| O7 | LP (2) | 1.98079 | C5–O6 | π* | 0.00001 | 60.46 | 0.34 | 0.129 |
| O8 | LP (1) | 1.97921 | C4 | | | 15.82 | 1.88 | 0.154 |
| O8 | LP (1) | 1.97921 | C4 | | 0.00068 | 1.42 | 3.38 | 0.062 |
| O8 | LP (1) | 1.97921 | C4 | | 0.00028 | 0.76 | 1.86 | 0.034 |
| O8 | LP (1) | 1.97921 | O8 | | | 0.55 | 1.81 | 0.028 |
| O8 | LP (1) | 1.97921 | O3–C4 | σ* | 0.00018 | 1.65 | 1.14 | 0.039 |
| O8 | LP (1) | 1.97921 | C4–C5 | σ* | 0.00008 | 1.33 | 1.04 | 0.034 |
| O8 | LP (2) | 1.98073 | C4 | | | 3.12 | 1.59 | 0.065 |
| O8 | LP (2) | 1.98073 | C4 | | 0.01155 | 0.89 | 2.15 | 0.04 |
| O8 | LP (2) | 1.98073 | O3–C4 | σ* | 0.00018 | 26.77 | 0.69 | 0.124 |
| O8 | LP (2) | 1.98073 | C4–C5 | σ* | 0.00008 | 21.87 | 0.59 | 0.102 |
| O8 | LP (2) | 1.98073 | C5–O6 | σ* | 0.00002 | 0.56 | 0.82 | 0.02 |
| C4–C5 | σ* | 0.00008 | C4 | | | 0.58 | 1 | 0.081 |
| C4–C5 | σ* | 0.00008 | C4 | | 0.00376 | 1.11 | 0.83 | 0.108 |
| C4–C5 | σ* | 0.00008 | C4 | | 0.00105 | 0.84 | 0.8 | 0.092 |
| C4–C5 | σ* | 0.00008 | C5 | | 0.00381 | 0.5 | 1.35 | 0.092 |
| C4–C5 | σ* | 0.00008 | O3–H9 | σ* | 0.00009 | 3.98 | 0.04 | 0.044 |
| C4–C5 | σ* | 0.00008 | O7–H10 | σ* | 0.00319 | 3.38 | 0.02 | 0.03 |
| C4–O8 | π* | 0.00005 | C4 | | | 1.55 | 1.59 | 0.13 |
| C4–O8 | π* | 0.00005 | C4 | | 0.00035 | 0.84 | 1.02 | 0.078 |
| C4–O8 | π* | 0.00005 | O8 | | 0.00001 | 1.27 | 0.62 | 0.074 |
| C5–O6 | π* | 0.00001 | C5 | | 0.00001 | 1.63 | 1.6 | 0.129 |
| C5–O6 | π* | 0.00001 | O6 | | | 1.3 | 0.5 | 0.065 |
| C5–O6 | π* | 0.00001 | C4–O8 | π* | 0.00005 | 68 | 0.02 | 0.074 |

[a] $E^{(2)}$ is the energy of the hyper conjugative interaction (stabilization energy).
[b] Energy difference between donor and acceptor i and j NBO orbitals.
[c] F (i,j) is the Fock matrix element between i and j NBO orbitals.

transformed to Raman intensities. The vibrational modes were assigned in accordance to the PED contributions evaluated with the Vibrational Energy Distribution Analysis (VEDA 4) program and are tabulated in Table 3. The wavenumbers calculated by B3LYP/LanL2DZ were scaled in FTIR and Raman by 1, 0.98 and 0.85 in the ranges of [2000–1407] $cm^{-1}$, [1406–341] $cm^{-1}$ and [340–0] $cm^{-1}$ [22].

To associate the title compound's measured vibrational frequencies with the values obtained through experiment, the Root Mean Square (RMS) value was computed by adopting Eq. (1) [23].

$$RMS = \sqrt{\frac{1}{n}\sum_{i}^{n}\left(\gamma_{i\,cal} - \gamma_{i\,exp}\right)^{2}} \quad (1)$$

FT-IR and FT-Raman bands in Figures 6 and 7 show an RMS value of 35.0890 $cm^{-1}$ and 25.7447 $cm^{-1}$ respectively. Figures 7 and 8 shows the correlation graphs obtained from the computed theoretical and observed experimental IR and Raman spectra of SO compound. The correlation coefficient ($R^2$) of experimental and calculated FT-IR and FT-Raman bands frequencies were found to be 0.99886 and 0.9974 respectively.

The peaks seen at 1630 $cm^{-1}$ and 1315 $cm^{-1}$ in FTIR and 1606 $cm^{-1}$ and 1314 $cm^{-1}$ in FT Raman corresponds to the O–C stretching vibrations mode of SO compound. This value is theoretically computed in the region 1602 $cm^{-1}$ (94%) and 1362 $cm^{-1}$. These regions firmly agree with the experimental data. The experimental frequency assigned to C–C stretching vibrations are seen in the region 512 $cm^{-1}$ and 490 $cm^{-1}$ in

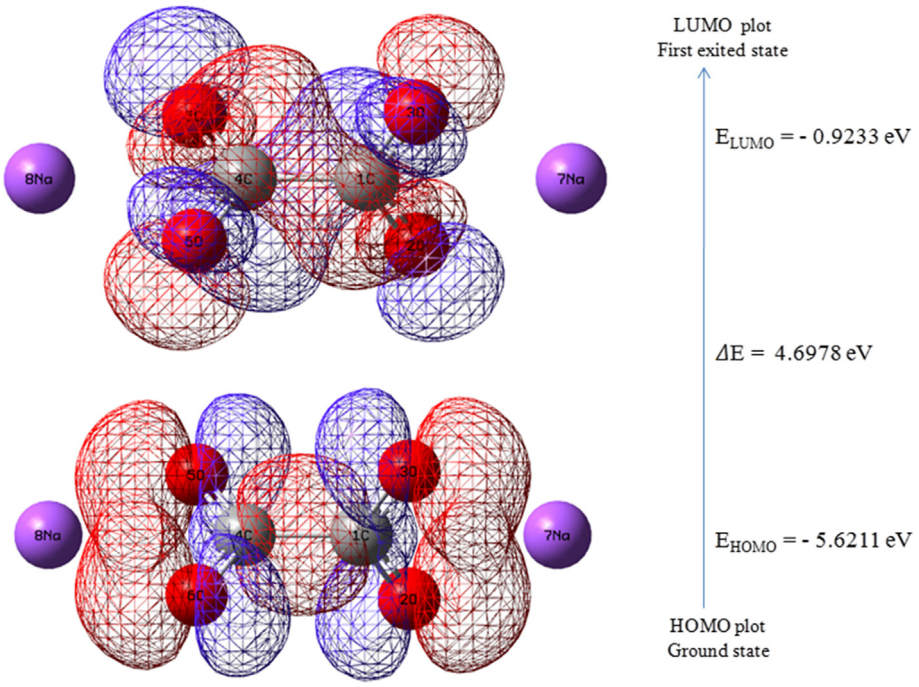


**Figure 9.** Frontier molecular orbital for SO.

both FTIR and FT Raman spectrum analysis respectively. These peaks were theoretically estimated at 52 $cm^{-1}$. The PED corresponding to this C–C vibration provides 27%. In the FT Raman spectrum, the peak at 159 $cm^{-1}$ were due to CCO bending vibration. This peak was theoretically recorded at 173 $cm^{-1}$ with PED value of (13%). The FTIR and Raman bands observed at 772 $cm^{-1}$ and 809 $cm^{-1}$ were assigned to the OCO bending vibration. Theoretically this is computed with wavenumber 805 $cm^{-1}$ with maximum PED value of 88%.

The NaOC bending vibration of the title compound is attributed to the peak at 210 $cm^{-1}$ and 159 $cm^{-1}$ in FT Raman Spectrum. Theoretically this is in agreement with the vibration at 212 $cm^{-1}$ (28%) and 173 $cm^{-1}$ (42%). From the FT Raman spectrum we see that SO shows OCC bending vibration at 893 $cm^{-1}$ and 159 $cm^{-1}$. Theoretically these vibrations were recorded at 870 $cm^{-1}$ (10%) and 204 $cm^{-1}$ (14%). The Raman bands observed at 89 $cm^{-1}$ is assigned to the torsion vibrations OCCO. This is theoretically computed from the wave number 66 $cm^{-1}$ with highest PED contributions of 100%.

The NaO stretching vibration is observed at 512 $cm^{-1}$ and 490 $cm^{-1}$ in FTIR and Raman spectrum with the corresponding theoretical value of 522 $cm^{-1}$ along with PED 20%. Identification of other vibrations like COOC and OCOC out of plane bending were observed at 893 $cm^{-1}$ in FT Raman analysis. Theoretically these were assigned at 870 $cm^{-1}$ with corresponding PED value of 33% and 36%. The average maximum potential energy of SO compound is 34.47%.

### 3.3. Frontier molecular orbitals

The molecular interactions that occur with various species can be found from the highest occupied molecular orbital (HOMO) which act as an electron donor and the lowest unoccupied molecular orbital (LUMO) that act as an electron acceptor. The energy related to HOMO is the potential for ionization, and that of LUMO is the attraction of the electrons. The difference in energy observed between HOMO and LUMO called band gap energy remains vital in determining the molecule's chemical stability and reactivity [24]. The HOMO and LUMO vitality give details on the possible charge move communications occurring inside the molecule.

The global molecular reactivity descriptors evaluated from the HOMO and LUMO energy values which are the ionization potential (IP), electron affinity (EA), electronegativity (χ), hardness (η), softness (S), chemical potential (μ) and electrophilicity index (ω) anticipated for the grown SO crystal are given in Table 4. The electrophilicity is a noteworthy property which is a proportion of the particle to acknowledge the electrons. Nucleophilicity is a measure of the molecule to contribute the electrons. Therefore, the electrophilicity and nucleophilicity of an atom impact the electronic property of the atom. Molecule with high value of electrophilicity is a poor donor and the molecule will be a good donor if it has a higher nucleophilicity. The ionization potential directly measures the reactivity of a compound, whereas the property of hardness and softness implies the stability of the compound. The estimated ionization potential value of 5.62 eV is the energy required to extract an electron from the HOMO. The measured lower value of 0.92 eV electron affinity bring to light that the grown SO crystal instantly accepts electrons in order to form bonds. This also implies that the reactivity with nucleophiles is high.

The simulated Frontier Molecular orbital for SO shown in Figure 9 indicates the existence of intramolecular charge transfer within the molecule. The measured band gap energy value of 4.7eV affirms that the molecule has stable structure and this value is comparable to that of other bioactive molecules [25].

### 3.4. Natural bond orbital analysis (NBO)

Study on the natural bond orbital (NBO) helps to explore the transfer of charge or conjugative interaction in a molecular system and provide knowledge on various hyper conjugative interactions and transfer of intermolecular charge between bonding and antibonding orbitals. To understand the intramolecular, rehybridization and delocalization of electron density observed in the molecule, NBO analysis was done on the title compound at B3LYP/6-311++G (d,p) level. The hyper conjugative interaction energy was presumed using the second order perturbation approach. For each donor NBO (i) and acceptor NBO (j) the stabilization energy $E^{(2)}$ related with electron delocalization amidst the donor and acceptor is computed using Eq. (2)

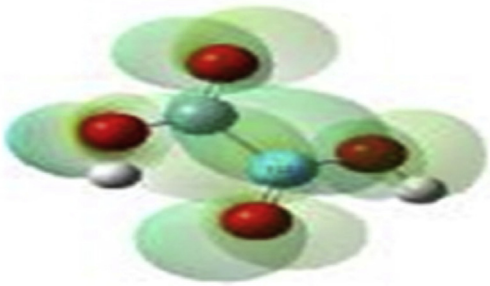

Figure 10. MEP map of SO.

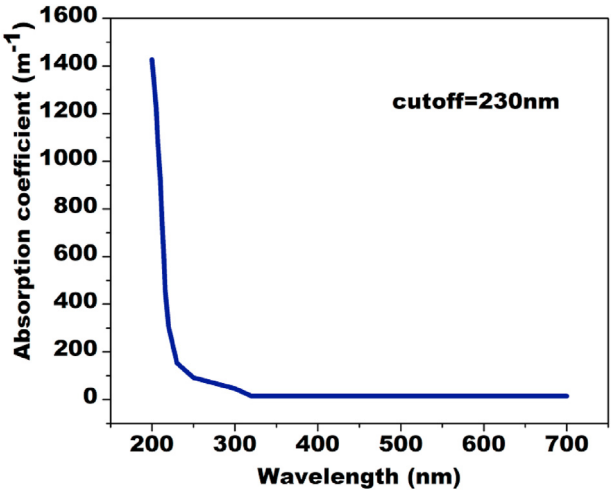


Figure 11. UV-Vis spectrum of SO.

$$E^{(2)} = \Delta E_{ij} = q_i \frac{F(i,j)^2}{E_i - E_j} \quad (2)$$

here qi represents the donor orbital occupancy, $E_j$ and $E_i$ are the diagonal elements and F (i,j) denotes the off diagonal NBO Fock matrix element [26]. Greater the interaction between the electron donors at high $E^{(2)}$ value, more intense is the interaction among electron donors and the degree to which the entire system conjugate increases [27]. Also, the intramolecular hyper conjugative interaction from $\sigma(O_3–H_9)$ to $\sigma^*(C_4–O_8)$ leads to 6.12 kcal/mol of stabilizing energy. Moreover, SO compound has hyper conjugative effect from the different bonds.

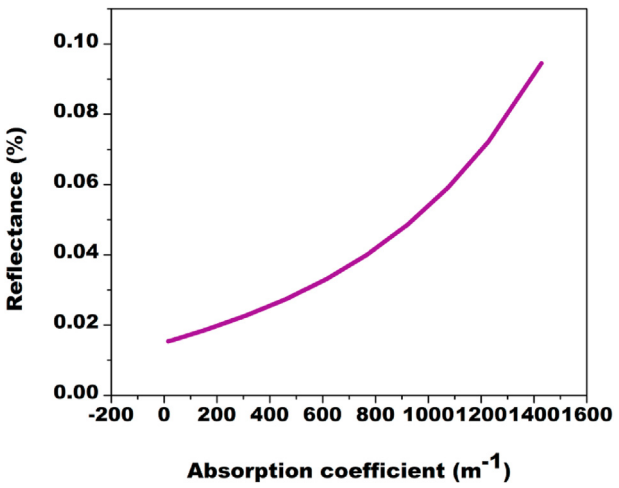


Figure 13. Dependence of reflectance on absorption coefficient for SO.

Interaction occurring from $\pi(C_4–O_8)$ to $\pi^*(C_5–O_6)$ contributes to 6.65 kcal/mol of stabilizing energy. The additional observable interaction arising from the resonance in the molecule were the electron is donated from the LP (2)$O_7$ to the electron from the antibonding $\pi^*(C_5–O_6)$ give a moderate stabilization energy of 60.46 kcal/mol and the details are given in Table 5.

### 3.5. Molecular Electrostatic Potential (MEP)

Molecular Electrostatic Potential (MEP) offers a complete description of the distribution of electron density around the molecule. This electron density specifically reflects the areas within the molecule of electrophilic and nucleophilic sites that are product of the compound's intermolecular interaction with the targets. To determine the reactivity sites for SO's nucleophilic and electrophilic attack, MEPs were obtained at the B3LYP/6-311++G (d,p) optimized geometry by adopting the Gauss View 5.0 [28] and the mapping obtained is presented in Figure 10. Various colours seen in the mapping reflect the number of electrons on the atomic sites. Red colour is more negative while white is more positive. The red area displays the region of greater electronegative electrostatic potential; blue denotes area with most electropositive electrostatic potential; and the zero-potential zone is indicated by green. The electron density varies as red > green > blue > pink > white. It is well evident from the map that regions which are electron rich are situated on atoms of Nitrogen and that regions with major electron deficient are positioned over the

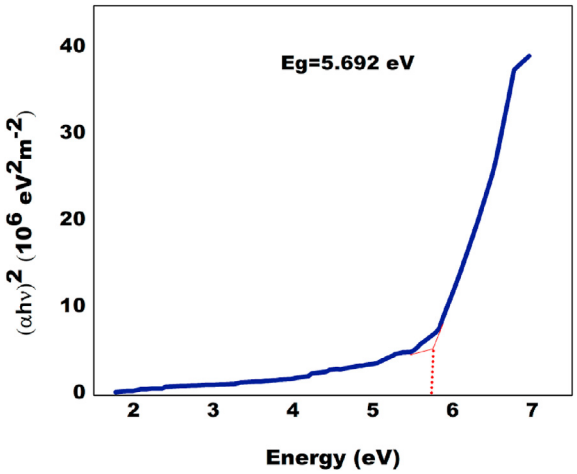


Figure 12. Plot of energy versus $(\alpha h\gamma)^2$ for SO.

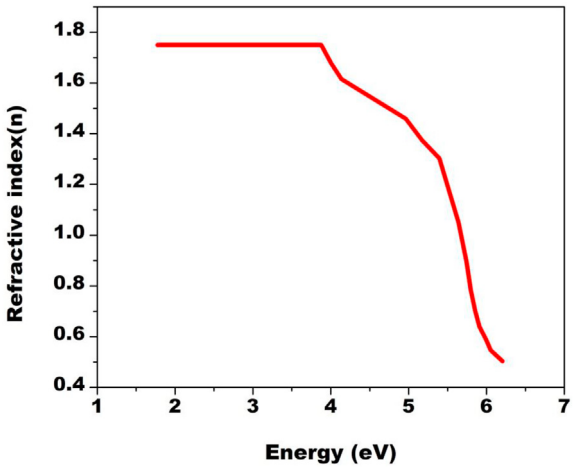


Figure 14. Energy dependence of refractive index for SO.

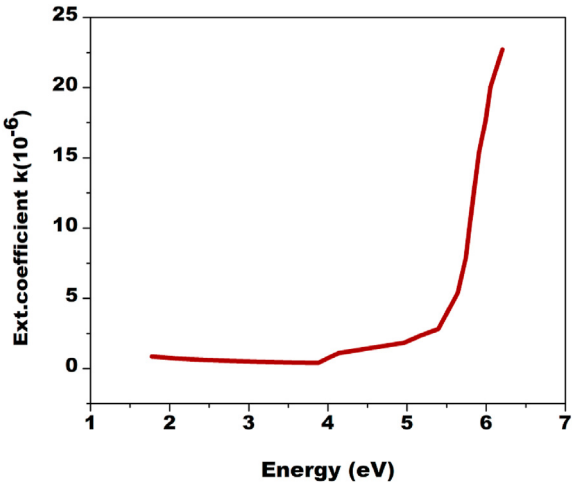


**Figure 15.** Dependence of extinction coefficient on energy for SO.

hydrogen atoms. These active sites in SO compound is found to provide an explicit evidence of biological activity.

### 3.6. UV-visible spectral analysis

UV-visible spectrum of grown SO crystal was taken in the region of wavelength 200–800 nm using LAMBDA-35UV-visible spectrophotometer. Figure 11, the UV-visible spectrum of SO reveal that there is no substantial absorption throughout the visible region and crystal is translucent in the entire visible range with cut off wavelength of 230 nm. This is one of the significant properties which supports the process of second harmonic generation. The material's optical band gap ($E_g$) is greatly connected with its atomic and electronic band structures and this significance make it suitable for electro-optic applications [29]. The bandgap energy $E_g$ for small photon energy hγ can be calculated by using Eq. (3)

$$(\alpha h\gamma)^n = A(h\gamma - E^t) \tag{3}$$

here A indicate the disorder parameter, h refers to Planck's constant, γ represent frequency of the incident photon and n indicates the nature of transition. $E^t = E_g$ for direct transition.

The bandgap of SO crystals was assessed by extrapolating a line on the x-axis in Figure 12, the Tauc's plot. The measured bandgap energy of 5.69eV shows that the grown SO crystals have large optical band gap and can be used effectively for applications with UV tunable lasers and NLO devices.

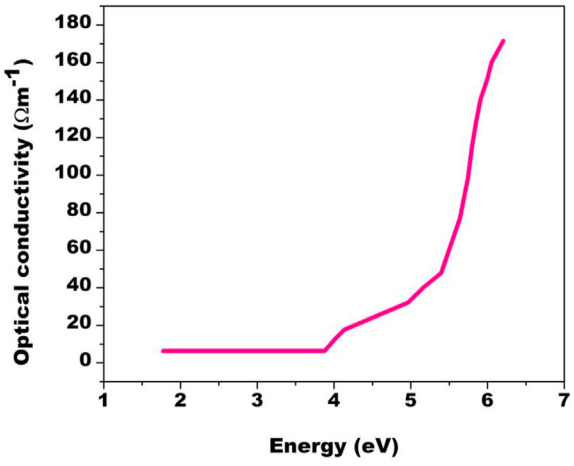


**Figure 16.** Plot of optical conductivity with energy for SO.

### 3.7. Estimation of optical constants

Constants like reflectance, extinction coefficient, optical conductivity and refractive index were computed by using the absorption data [30]. Absorption coefficient (α) and extinction coefficient (k) is connected by the relation given in expression (4)

$$k = \frac{\alpha\lambda}{4\pi} \tag{4}$$

The expression connecting reflectance (R), optical absorption coefficient (α) and refractive index ($n_x$) [31] is given as Eqs. (5) and (6).

$$R = 1 \pm \frac{\sqrt{1 - \exp(-\alpha t) + \exp(\alpha t)}}{1 + \exp(-\alpha t)} \tag{5}$$

$$n_x = -\left\{\frac{(R+1) \pm \sqrt{3R^2 + 10R - 3}}{2(R-1)}\right\} \tag{6}$$

It is evident from the graph shown in Figure 13 that there is a rise in the percentage of reflectance with increase in absorption coefficient and also that the reflectance depends on the absorption coefficient.

Materials suitable for the optoelectronic devices can be produced by effectively adjusting the energy of the incident photon because the incident photon energy affects the performance of the device. The linear refractive index (n) evaluated from Figure 14, the dependence of refractive index and energy bandgap is 1.710 for SO crystal at 310 nm. Refractive index is known to decrease with energy gap. Higher band gap materials in general have lower refractive index. The dependency of refractive index with energy gap obeys the Moss relation or Ravindra relation in most cases and it depends on the material's nature [32]. However, the observed constant refractive index up to 3.8eV may be due to the anomalous dispersion due to dielectric relaxation at lower frequencies.

The higher optical clarity and lower refractive index shown by SO single crystals in UV region makes SO as a remarkable candidate suiting to behave as antireflective coating in solar thermal devices and NLO applications [33]. The graph of variation in extinction coefficient in response to energy given in Figure 15 shows that the rate of extinction coefficient depends on high energy from photon.

The photonic exchange caused due to optical conductivity ($\sigma_{op}$) of a sample when it is irradiated with light is given by Eq. (7)

$$\sigma = \frac{n_x \alpha c}{4\pi} \tag{7}$$

From the graph shown in Figure 16 the plot of optical conductivity with photon energy, it is seen that there is an increase in optical conductivity with photon energy and this behavior reflects the existence of high photo tunable property in SO [34].

### 3.8. Thermodynamic calculations

Investigations on the thermodynamic properties of a material stays extremely important while choosing a material for use at high temperature and pressure [35]. Thermodynamic functions like heat capacity (Cp) entropy (S) and enthalpy changes (H) of SO crystal was calculated using DFT/B3LYP/6-311++G (d,p) method and are furnished in Table 6. Such energies are extremely helpful in ascertaining the direction of chemical reactions in line with the 2nd law of thermodynamics [36]. It is well understood from Table 6 that there is an increase in thermodynamic functions with increase of temperature. This increase is because there is a rise in the intensities of molecular vibration with increase in temperature. The entropy is the indicator of the compound disorder lines and it is found that the entropy increases with temperature rise due to thermal

**Table 6.** Thermodynamic functions of the title compound.

| T (K) | S (J/mol.K) | Cp (J/mol.K) | ddH (kJ/mol) |
|---|---|---|---|
| 100 | 291.966 | 74.785 | 5.448 |
| 200 | 352.825 | 101.618 | 14.382 |
| 298 | 396.902 | 119.498 | 25.275 |
| 300 | 397.642 | 119.79 | 25.496 |
| 400 | 434.09 | 133.669 | 38.199 |
| 500 | 465.114 | 144.302 | 52.122 |
| 600 | 492.168 | 152.33 | 66.973 |
| 700 | 516.124 | 158.359 | 82.522 |
| 800 | 537.581 | 162.911 | 98.596 |
| 900 | 556.979 | 166.386 | 115.068 |
| 1000 | 574.655 | 169.074 | 131.847 |

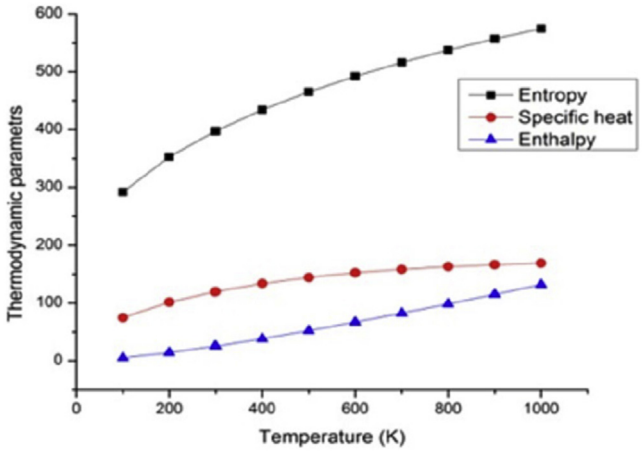


**Figure 17.** Correlation plot of thermodynamic properties of the title compound.

agitation. The specific heat capacity which is the measure of how efficiently the material stores energy also increases with temperature.

The equations connecting the heat capacity, entropy, enthalpy changes and temperatures of SO were fitted by using the quadratic formulae. The corresponding fitting factors ($R^2$) for these thermodynamic properties are 0.99313, 0.99681 and 0.99963 respectively and the fit equations are given as expressions (8), (9) and (10). The correlation graphs are shown in Figure 17.

$$Cp = 54.16715 + 0.25686T–1.49874 \times 10^{-4}T^2R^2 = 0.99313 \quad (8)$$

$$S = 244.07332 + 0.57531T–2.58526 \times 10^{-4}T^2R^2 = 0.99681 \quad (9)$$

$$H = -4.81212 + 0.08772T + 5.14917\times10^{-5}T^2\ R^2 = 0.99963 \quad (10)$$

### 3.9. Topology analysis

The topology analysis was carried out using Electron localization function (ELF) along with Localized orbital locator (LOL) maps. Multiwin program was executed based on the covalent bond. From these maps it is

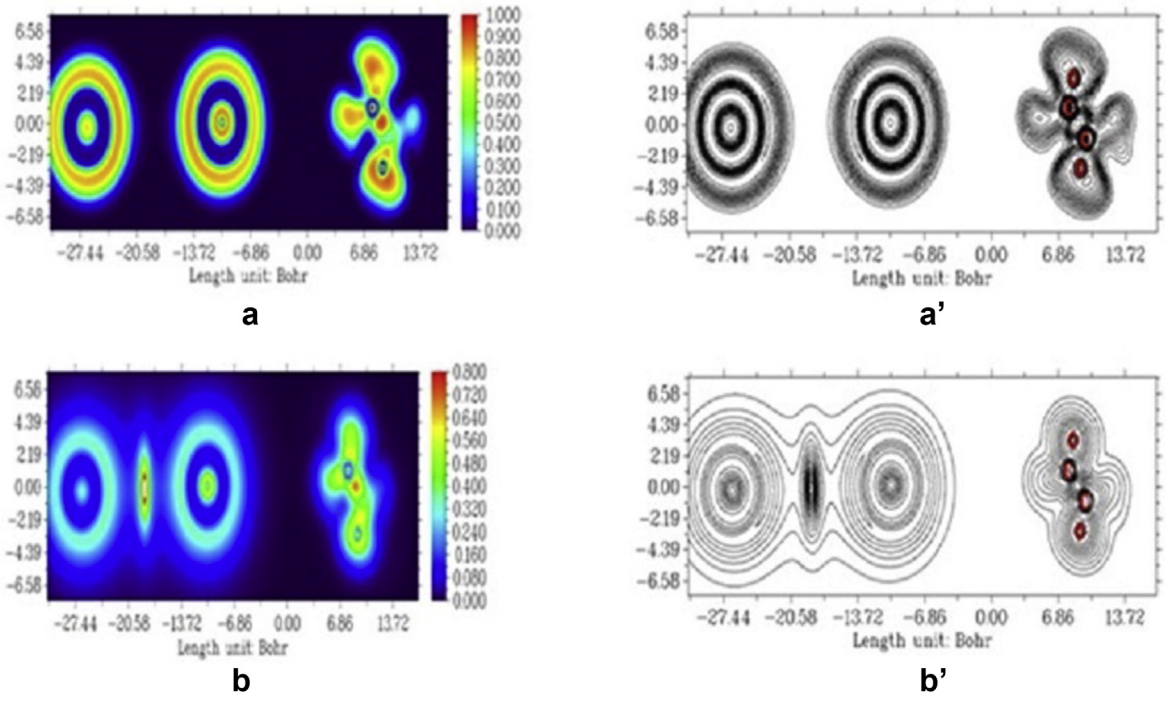


**Figure 18.** (a)& (a') ELF, colour filled and contour map of the title compound, (b)&(b') LOL colour filled and contour c map of the title compound.

**Table 7.** Mulliken charge distribution, Fukui function and local softness of SO.

| Atoms | Mulliken atomic charges | | | Fukui functions | | | | Local softness | | | |
|---|---|---|---|---|---|---|---|---|---|---|---|
| | N | N +1 | N-1 | $fr^{+}$ | $fr^{-}$ | $fr^{0}$ | Δf(r) | $S_k^{+}$ | $S_k^{-}$ | $S_k^{0}$ | ΔSk |
| Na1 | -0.00273 | -0.392381 | 0.497115 | -0.389652 | -0.49984 | -0.44475 | 0.110192 | -0.08148 | -0.10452 | -0.093 | 0.023041 |
| Na2 | 0.003269 | -0.286383 | 0.503407 | -0.289652 | -0.50014 | -0.3949 | 0.210486 | -0.06057 | -0.10458 | -0.08257 | 0.044013 |
| O3 | -0.06954 | -0.099555 | -0.076153 | -0.030017 | 0.006615 | -0.0117 | -0.03663 | -0.00628 | 0.001383 | -0.00245 | -0.00766 |
| C4 | 0.088376 | 0.063071 | 0.087239 | -0.025305 | 0.001137 | -0.01208 | -0.02644 | -0.00529 | 0.000238 | -0.00253 | -0.00553 |
| C5 | 0.155088 | 0.105217 | 0.157038 | -0.049871 | -0.00195 | -0.02591 | -0.04792 | -0.01043 | -0.00041 | -0.00542 | -0.01002 |
| O6 | -0.36721 | -0.44217 | -0.367521 | -0.074959 | 0.00031 | -0.03732 | -0.07527 | -0.01567 | 6.48E-05 | -0.0078 | -0.01574 |
| O7 | -0.08534 | -0.115991 | -0.083366 | -0.030651 | -0.00197 | -0.01631 | -0.02868 | -0.00641 | -0.00041 | -0.00341 | -0.006 |
| O8 | -0.28432 | -0.362764 | -0.281545 | -0.078443 | -0.00278 | -0.04061 | -0.07567 | -0.0164 | -0.00058 | -0.00849 | -0.01582 |
| H9 | 0.253301 | 0.246192 | 0.251297 | -0.007109 | 0.002004 | -0.00255 | -0.00911 | -0.00149 | 0.000419 | -0.00053 | -0.00191 |
| H10 | 0.309106 | 0.284765 | 0.312488 | -0.024341 | -0.00338 | -0.01386 | -0.02096 | -0.00509 | -0.00071 | -0.0029 | -0.00438 |

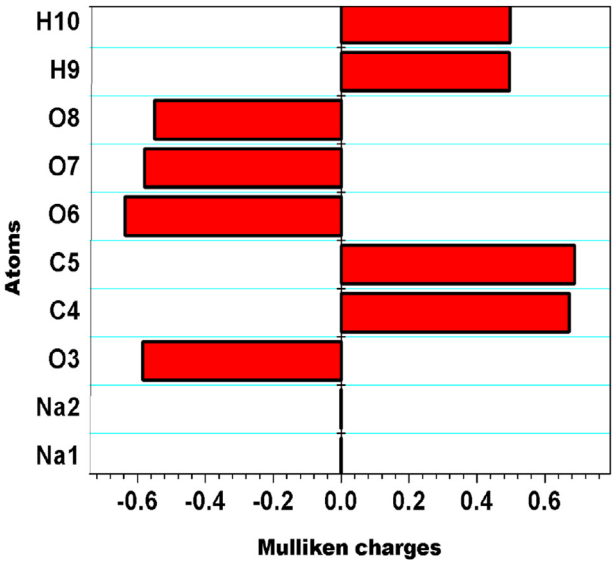


**Figure 19.** Mulliken population Analysis of SO compound.

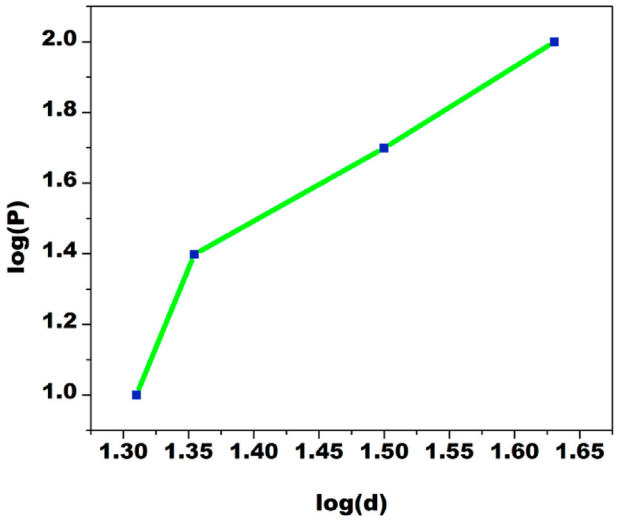


**Figure 21.** Variation of log P with log d.

able to find the place where the probability of identifying an electron pair is high. The high ELF value (approximately 0.8–1.0eV) are seen in red colour. The series go down through brown and yellow to green for middle ELF Value (approximately 0.5eV). The lower end is depicted in blue colour. The presence of a broad ELF and LOL value [37] in a region is due to existence of a covalent bond or a nuclear shell or a pair of lone electrons and indicate high localization of electrons. Figure 18 depicts the colour filled and contour map of ELF and LOL of the title compound. The red-coloured regions are due to the covalent bonds and has high LOL value. The electron depletion regions amongst the inner shell and the valence shell are exposed as blue circles around the nuclei. The blue circle region denotes negative sign of isosurface and thereby show a strong attractive interaction. Also, the area with low electron density which is similar to van der Walls interaction is assigned by green circle. The red or orange region represent strongest repulsive interaction between the atoms of SO compound.

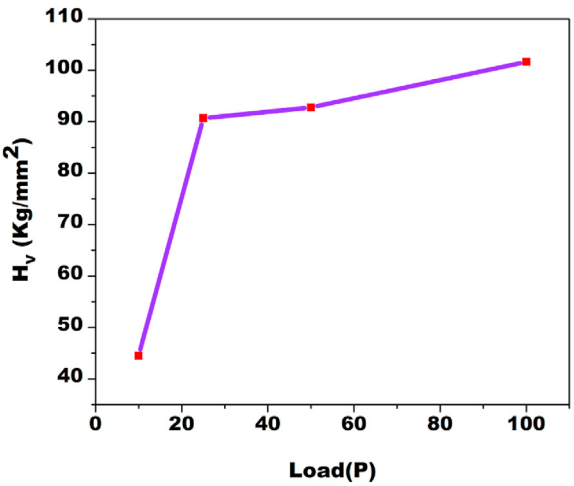


**Figure 20.** Dependence of hardness number on load for SO.

### 3.10. Fukui function descriptors analysis

The chemical and ionization potential is understood by the Mulliken atomic charge calculation and was done for SO because the atomic charge influences the dipole moment, polarizability, electronic structure and various other properties of the molecular system. This is a popularly used density functional descriptors to illustrate chemical reactivity and discrimination. Hence, by Mulliken population analysis (MPA) and Fukui function using B3LYP/6-311++G (d,p) method, the natural population analysis of SO was done. To compare the variance in the Mulliken charges, the charge and multiplicity are changed. When the number of electrons is refitted, the Fukui function descriptors will show the chosen areas where a chemical species will alter its density. Accordingly, it shows the competence of the electron density to deform from a given position by donating and accepting electrons [38, 39, 40]. Atomic Fukui function at the $r^{th}$ atomic site for an electrophilic $f^{-}(r)$, nucleophilic f

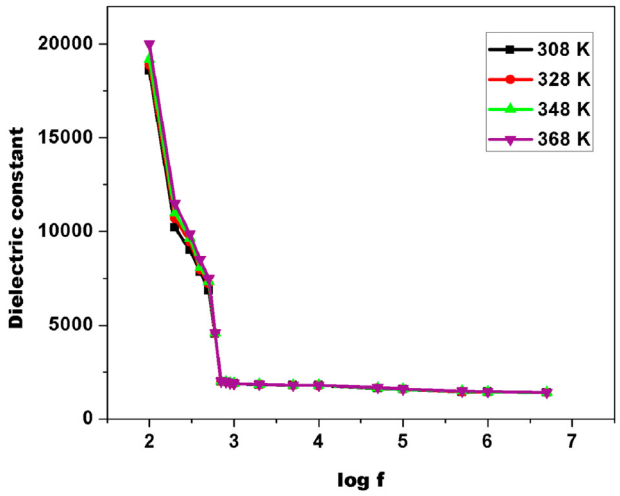


Figure 22. Dependence of dielectric constant of SO with log f.

$^{+}$(r), and free radical attack f $^{0}$(r) are calculated from Mulliken population analysis. Dual descriptors like Δf(r) and $\Delta S_{(k)}$ [41] are calculated by using the relations (11) and (12).

$$\Delta f(r) = f^{+}(r) - f^{+}(r) \tag{11}$$

$$\Delta S_{(k)} = S_k^{+} - S_k^{-} \tag{12}$$

For the site to have nucleophilic attack, Δf(r) > 0, whereas when Δf(r)<0 the site undergoes an electrophilic attack. $\Delta S_{(k)}$, the condensed version [42] of product of Δf(r) with the molecular softness (S). Table 7 exhibits the Mulliken atomic charge, Fukui function and local softness values of SO. Rendering to the dual descriptor conditions, the nucleophilic sites for SO are Na1and Na2. Similarly, the electrophilic sites are O8, O6, C5, O3, O7, C4, H10 and H9. Dual descriptor shows that the Na2 atom has higher positive value since they are more nucleophilic attack and O8 inhibit a high negative value of dual descriptor thereby indicate that they are more electrophilic attack. The distribution of atomic charges obtained for all the atoms using the Mulliken population analysis is shown in Figure 19. Almost maximum number of sodium atoms manifest positive charge naturally. However, maximum of carbon and oxygen atoms are negatively charged. Hence from the Fukui's concept of molecular orbital theory, it is very well understood that a most preferred exceptional electrophilic reaction in a molecule occurs in the area where

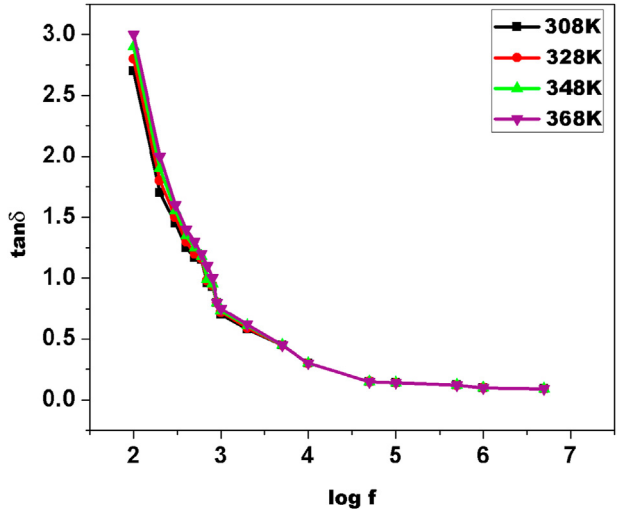


Figure 23. Dependence of tan $\delta$ of SO with log f.

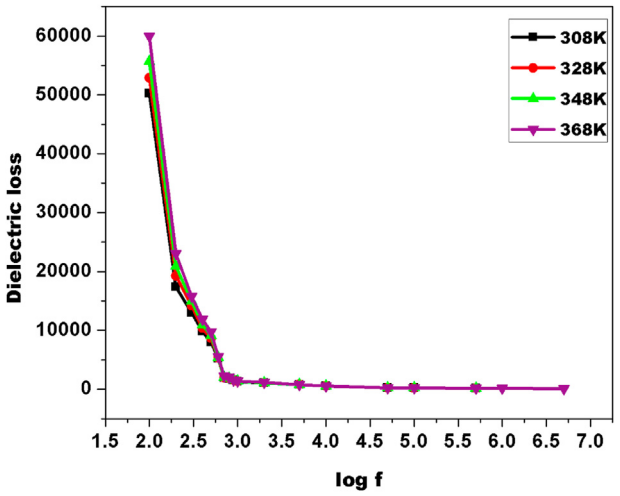


Figure 24. Plot of log f vs dielectric loss.

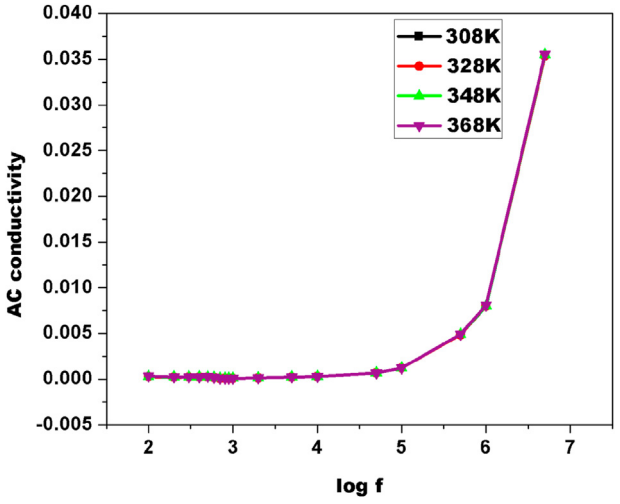


Figure 25. Plot of log f vs AC conductivity.

the relative density of the highest occupied molecular orbital (HOMO) is high. The environment which has a high lowest unoccupied molecular orbital (LUMO) density is due to the nucleophilic reaction.

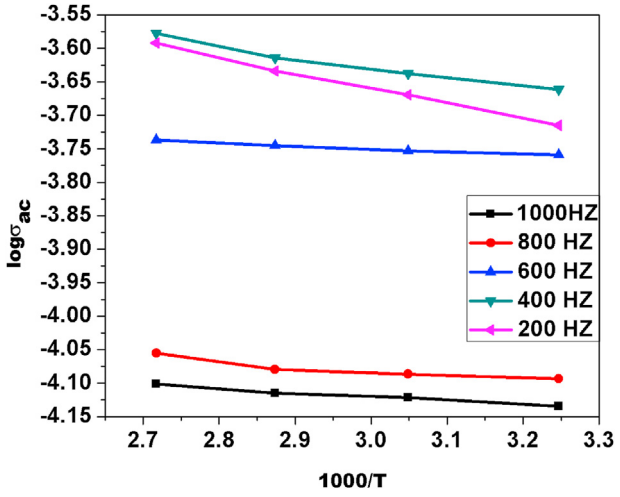


Figure 26. Plot of 1000/T vs log $\sigma_{ac.}$

**Table 8.** Activation energy values for different frequencies of SO.

| S.No | Frequency HZ | Activation Energy $E_{ac}$ (J) | Activation Energy $E_{ac}$ (ev) |
|---|---|---|---|
| 1 | 200 | 3.67356E-21 | 0.022931 |
| 2 | 400 | 3.24438E-21 | 0.020252 |
| 3 | 600 | 2.73102E-21 | 0.017048 |
| 4 | 800 | 2.16246E-21 | 0.013499 |
| 5 | 1000 | 1.23924E-21 | 0.007736 |

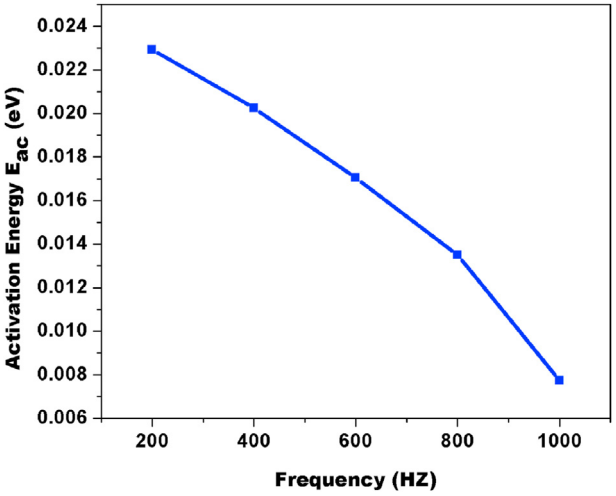


**Figure 27.** Plot of frequency vs Activation Energy $E_{ac.}$

### 3.11. Vickers micro hardness studies

The property of a material to resist deformation, indentation, or penetration when subjected to process like abrasion, drilling, impact, scratching, and/or wear is referred as its hardness and is measured by hardness tests. The key role in device fabrication is that the measured hardness number should be independent of the load applied [43]. Smooth and even surface of SO crystal was subjected to the hardness analysis in room temperature for a load ranging from 25 gm to 100 gm using a Vicker's Hardness tester. The hardness number ($H_v$) was computed by using the relation (13)

$$H_v = 1.8544p/d^2\ Kgmm^{-2} \tag{13}$$

here p refers to the load applied and d represents the diagonal length of the indented impressions. The plot of Hardness number versus applied load in Figure 20 show that the hardness number increases with increase in load. This rise in the hardness number with increase in load is due to the reverse indentation effect. Adopting the Meyer's relation given in Eqs. (14) and (15) the index coefficient was computed

$$P = K^1 d^n \tag{14}$$

$$P = \log K_1 + n\log d \tag{15}$$

Here $K_1$ the standard hardness was calculated from Figure 21, the graph of load P versus d. From the slope of the curve, the value of 'n' was determined using least square fit method and is found to be greater than 2. Hence the grown crystal is soft in nature.

### 3.12. Dielectric studies

The dielectric properties exhibited by solids give details about the electric fields within the solid and it is very important to understand clearly the electro-optic characteristics of these crystalline solids. Dielectric studies provide important information about the material's electrical properties and enable electrical fields to move through the crystalline solids [44]. The frequency dependence of the electrical properties gives a clear perception about the applications of materials. The dielectric measurement of the grown SO crystal was done using HIOKI 3532 LCR meter. A cut crystal of uniform cross section sample of SO electroded with silver paste was used for the measurement. The experiment was conducted out for frequencies varying from 50 Hz to 5 MHz and at 35 °C, 55 °C, 75 °C and 95 °C. The dielectric constant and dielectric loss of the crystals was determined using expressions (16) and (17).

$$\text{Dielectric constant } \varepsilon' = \frac{Ct}{A\varepsilon_0} \tag{16}$$

here C stands for the Capacitance in μF, t the thickness of specimen, A denotes the area of the sample in $mm^2$ and $\varepsilon_0 = 8.854 \times 10^{-12}\ Fm^{-1}$ is the permittivity of free space.

$$\text{Dielectric loss } \boldsymbol{\varepsilon}'' = \boldsymbol{\varepsilon}' \tan\delta \tag{17}$$

where $\tan\delta$ is the Dissipation factor.

The dependence of dielectric constant with frequency at different temperatures for SO is shown in Figure 22. The dielectric constant of a material depends mainly on four types of polarization which are ionic, electronic, orientation and space charge. At low frequency the value of dielectric constant was found to be high which is usually due to high polarization activity while the low polarization activity at higher frequencies results in a decrease of the dielectric constant of crystals [45]. This behavior obeys the Miller rule [46] i.e., with an increase in frequency there is an exponential decrease of dielectric constant. The high dielectric constant observed in SO is similar to that observed in Ammonium Oxalate [47] and Urea Oxalic acid crystal [34]. At very high frequency the dielectric constant was found to be constant. Also with the increase of temperature, the dielectric constant also increases. This observed change in value of dielectric constant with temperature can be attributed to the permanent dipole moment exhibited by orientation polarization.

The profile of dielectric loss of the crystal at different temperatures is plotted in Figure 23 and Figure 24. The low dielectric constant values with reduced dielectric loss at higher frequencies in SO crystal indicate improved optical efficiency with lesser defects [48, 49] and suggest utility for applications of optoelectronics devices.

The plot of ac conductivity as a function of frequency is shown in Figure 25. At higher frequencies the conductivity value is high fora given temperature that is caused by the hopping of the polaron in the crystals [50]. This rise in conductivity is due to the decrease in the space charge polarization at higher frequencies.

From the plot of conductivity (ln σ) versus temperature (1000/T) shown in Figure 26, the activation energy in terms of electrical performance for the SO crystal was calculated using Eqs. (18) and (19).

$$\sigma_{ac} = \sigma_0 \exp\left(\frac{E_a}{K_B T}\right) \tag{18}$$

where $\sigma_{ac}$- conductivity and $k_B$ indicate the Boltzman constant.

$$E_a = -slope \times 1000 \times K_B \quad (19)$$

The measured values of activation energies for different frequencies are tabulated in Table 8. A plot between the activation energies as a function of frequency (Figure 27) shows that at high frequency of charge carriers, the activation energy was found to be less which is due to the charge transport from defect position to the next position.

## 4. Conclusion

Transparent and good SO single crystals were grown by employing the slow evaporation solution growth technique. Functional groups found in SO were identified using FT-IR and FT-Raman spectral analysis. For the grown SO crystal detailed vibrational spectral analysis and DFT computations were performed. The calculated geometric parameters (bond lengths and bond angles) were determined theoretically and compared to the experimental values, and have been found to be in agreement. The notable difference in HOMO and LUMO energy supports the charge transfer model of interaction within the molecule. The NBO analysis revealed that there is an effective transfer of intramolecular charge within the molecule. The negative potential sites on oxygen and nitrogen atoms, and the positive potential sites on the title compound's NH hydrogen atoms were revealed by MEP map.

From UV-Vis spectral analysis we see that SO crystal is transparent throughout the visible region and has a cutoff wavelength of 230 nm. Also, the optical band gap energy is found to be 5.69 eV. The calculated thermodynamic properties such as Cp, S and H increases with increase in temperature which is associated with the enhancement of the molecular vibration. The topology analysis indicates electron attractive and repulsive sites in SO compound atoms from the maps of Electron localization function and Localized orbital locator. The Fukui concept of molecular theory implies that the title compound has more electrophilic attack which is due to high HOMO density. Microhardness test reveal the reverse indentation size behavior in SO thereby revealing its soft nature. The behaviour of SO at high frequencies exhibiting low dielectric constant and dielectric loss reveal that SO crystals can be used for electro-optic applications. The measured activation energies were lower at high frequency due to the transfer of charge from defect position to the next position.

## Declarations

### Author contribution statement

R. Ramalakshmi: Conceived and designed the experiments; Performed the experiments; Analyzed and interpreted the data; Wrote the paper.

S. Stella Mary: Conceived and designed the experiments; Contributed reagents, materials, analysis tools or data; Wrote the paper.

S. Shahil Kirupavathy: Analyzed and interpreted the data; Wrote the paper.

S. Muthu: Conceived and designed the experiments; Analyzed and interpreted the data.

Renjith Thomas: Contributed reagents, materials, analysis tools or data.

### Funding statement

This research did not receive any specific grant from funding agencies in the public, commercial, or not-for-profit sectors.

### Data availability statement

Data included in article/supplementary material/referenced in article.

### Declaration of interests statement

The authors declare no conflict of interest.

### Additional information

No additional information is available for this paper.

## Acknowledgements

The authors wish to express their gratitude to the authors D.A.Reed and M.M. Olmstead for the experimental data related to the crystal structure, space group, unit cell parameters and atomic coordinates that are cited in this article.

## References

[1] H.S. Nalwa, Organometallic materials for non linear optics, Appl. Organomet. Chem. 5 (1991) 349–377.
[2] D.S. Chemla, J. Zyss, Non Linear Optical Properties of Organic Molecules and Crystals, Academic Press, New York, 1987.
[3] Sachio Horiuchi, Reji Kumai, Yoshinori Tokura, Room-temperature ferroelectricity and gigantic dielectric susceptibility on a supramolecular architecture of phenazine and deuterated chloranilic Acid, J. Am. Chem. Soc. 127 (2005) 5010–5011.
[4] N.W. Smirnova, O.A. Petrii, A. Grzejdz, Effect of ad-atoms on the electro-oxidation of ethylene glycol and oxalic acid on platinized platinum, J. Electron. Chem. 251 (1988) 73–87.
[5] L. Eyring, Progress in the Science and Technology of the Rare Earths I, Pergamon press, New York, 1964.
[6] P. Rajesh, P. Ramasamy, Effect of oxalic acid on the optical, thermal, dielectric and mechanical behaviour of ADP crystals, Phys. B 404 (2009) 1611–1616.
[7] A. Moses Ezhil Raj, D. Deva Jayanthi, V. Bena Jothy, M. Jayachandran, C. Sanjeeviraja, Growth aspects of barium oxalate monohydrate single crystals in gel medium, Cryst. Res. Technol. 43 (12) (2008) 1307–1313.
[8] K.V. Bangera, P. Mohan Rao, Growth and characterization of single crystals of Barium ammonium oxalate in silica hydrogel, Indian J. Pure Appl. Phys. 32 (1994) 871.
[9] B.P. Agarwal, K.M. Chauhan, Mohan M. Bhadbhade, Growth and characterization of cadmium oxalate crystals using agar gel, Indian J. Pure Appl. Phys. 37 (1999) 395–398.
[10] Yuniar Ponco Prananto, Mohammad Misbah Khunur, Dini Tri Wahyuni, Rizky Arief Shobirin, Yoga Rizky Nata, Efiria Riskah, Study of gel growth cobalt(II) oxalate crystals as precursor of CO3O4 nano particles, Bull. Chem. React. Eng. Catal. 7 (3) (2013) 198–204.
[11] B.B. Parekh, P.M. Vyas, Sonal, R. Vasant, M.J. Joshi, Thermal, FT-IR and dielectric studies of gel grown sodium oxalate single crystal, Bull. Mater. Sci. 31 (2) (April 2008) 143–147.
[12] F. Colmenero, V. Timón, Study of the structural, vibrational and thermodynamic properties of natroxalate mineral using density functional theory, J. Solid State Chem. 263 (2018) 131–140.
[13] K.I. Peterson, D.P. Pullman, Determining the structure of oxalate anion using Infrared and Raman spectroscopy coupled with Gaussian calculations, J. Chem. Educ. 93 (2016) 1130–1133.
[14] R.L. Frost, J. Yang, Z. Ding, Raman and FTIR spectroscopy of natural oxalates implications for the evidence of life on Mars, Chin. Sci. Bull. 48 (2003) 1844–1852.
[15] M.J. Frisch, G.W. Trucks, H.B. Schlegel, G.E. Scuseria, M.A. Robb, J.R. Cheeseman, G. Scalmani, V. Barone, B. Mennucci, G.A. Petersson, H. Nakatsuji, M. Caricato, X. Li, H.P. Hratchian, A.F. Izmaylov, J. Bloino, G. Zheng, J.L. Sonnenberg, M. Hada, M. Ehara, K. Toyota, R. Fukuda, J. Hasegawa, M. Ishida, T. Nakajima, Y. Honda, O. Kitao, H. Nakai, T. Vreven, J.A. Montgomery Jr., J.E. Peralta, F. Ogliaro, M. Bearpark, J.J. Heyd, E. Brothers, K.N. Kudin, V.N. Staroverov, R. Kobayashi, J. Normand, K. Raghavachari, A. Rendell, J.C. Burant, S.S. Iyengar, J. Tomasi, M. Cossi, N. Rega, J.M. Millam, M. Klene, J.E. Knox, J.B. Cross, V. Bakken, C. Adamo, J. Jaramillo, R. Gomperts, R.E. Stratmann, O. Yazyev, A.J. Austin, R. Cammi, C. Pomelli, J.W. Ochterski, R.L. Martin, K. Morokuma, V.G. Zakrzewski, G.A. Voth, P. Salvador, J.J. Dannenberg, S. Dapprich, A.D. Daniels, O. Farkas, J.B. Foresman, J.V. Ortiz, J. Cioslowski, D.J. Fox, Gaussian Inc Wallingford, CT, 2009.
[16] M. Raja, R. Raj Muhamed, S. Muthu, M. Suresh, Synthesis, Spectroscopic (FT-IR, Ft-Raman, NMR. UV-Visible), Fukui Function, antimicrobial and molecular docking study of (E)-1(3-bromobenzylidence) semicarbazide by DFT method, J. Mol. Struct. 1130 (2017) 374–384.
[17] M.H. Jamroz, Vibrational Energy Distribution Analysis 4, VEDA, Warsaw, 2004.
[18] G. Rauhut, P. Pulay, Transferable scaling factors for density functional derived vibrational force fields, J. Phys. Chem. 99 (1995) 3093–3100.
[19] I. Sidir, Y.G. Sidir, M. Kumalar, E. Tasal, Ab initio Hartee-Fock and density functional theory investigation on the conformational stability, molecular structure and vibrational spectra of 7-acetoxy-6-(2,3-dibromopropyl)-4,8-dimethlcoumarin molecule, J. Mol. Struct. 964 (2010) 134–151.
[20] G.A. Jeffrey, G.S. Parry, The crystal structure of sodium oxalate, J. Am. Chem. Soc. 76 (1954) (1954) 5283.

[21] D.A. Reed, M.M. Olmstead, Sodium oxalate structure refinement, Acta Crystallogr. B37 (1981) 938–939.
[22] A. Abkari, I. Chaabane, K. Guidara, DFT (B3LYP/LanL2DZ and B3LYP/6311G +(d,p)) comparative vibrational spectroscopic analysis of organic-inorgonic compound bis(4-acetylanilinium) tetrachlorocuprate(II), Physica E 81 (2016) 136–144.
[23] Z. Rui-Zhou, Z. Xian-Zhou, Molecular structure, NMR parameters, IR spectra of *N*-(1,3,4-thiadiazol-2-yl)-1-[1-(6-chloropyridin-3-yl)methy]-5-methyl-1*H*-[1,2,3] triazol-4-carboxamide by density functional theory and *ab-initio* Hartree-Fock calculations Indian, J. Pure Appl. Phys. 51 (2013) 164.
[24] I. Fleming, Frontier Orbitals and Orbital Chemical Reactions, John Wiley and Sons, New York, 1976.
[25] O. Tamer, B. Sariboga, Ibrahim Ucar, A combined crystallographic, Spectroscopic, antimicrobial and computational study of novel dipicolinate copper (II) complex with 2-(2-hydroxyethyl) pyridine, Struct. Chem. 23 (2012) 659–670.
[26] H. Pir, N. Gunay, O. Tamer, D. Avcı, Y. Atalay, Theoretical investigation of 5-(2 Acetoxyethyl)-6-methylpyrimidin-2,4-dione: conformational study, NBO and NLO analysis, molecular structure and NMR spectra, Spectrochem. Acta Part A Mol. Biomol. Spectrosc. 112 (2013) 331e342.
[27] Tintu K. Kuruvilla, Johanan Christian Prasana, S. Muthu, Jacob George, Vibrational spectroscopic (FT-IR,FT-Raman) and quantum mechanical study of 4-(2-chlorophenyl)-2-ethyl-9-methyl-6H-thieno[3,2-f][1,2,4]triazolo[4,3-a][1,4] diazepine, J. Mol. Struct. 1157 (2018) 519–529.
[28] Roy Dennington Todd Keith, John Millam, Gauss View, Semichem Inc., Shawnee Mission, K.S, 2009 version 5.
[29] V. Krishna Kumar, L. Guru Prasad, R. Nagalakshmi, Investigation on 3-aminophenol: a non linear optical crystal for frequency doubling, Eur. Phys. J. Appl. Phys. 48 (2009) 20403–20409.
[30] P.V. Dhanaraj, T. Suthan, N.P. Rajesh, Synthesis, crystal growth and characterization of a semiorganic material: calcium dibromide bis(glycine) tetrahydrate", Curr. Appl. Phys. 10 (2010) 1349–1353.
[31] R. Surekha, R. Gunaseelan, P. Sagayaraj, K. Ambujam, L-Phenylalanine L-phenylalaninium bromide – a new nonlinear optical material, R. Soc. Chem. Cryst. Eng. Comm. 16 (2014) 7979–7989.
[32] N.M. Ravindra *, Preethi Ganapathy, Jinsoo Choi, Energy gap–refractive index relations in semiconductors – an overview, Infrared Phys. Technol. 50 (2007) 21–29.
[33] V. Sangeetha, K. Gayathri, P. Krishnan, N. Sivakumar, N. Kanagathara, G. Anbalagan, Growth, optical, thermal, dielectric and microhardness characterizations of melaminium bis (trifluoroacetate) trihydrate single crystal, J. Cryst. Growth 389 (2014) 30–38.
[34] S. Jeeva, S. Muthu, S. Tamilselvan, M. Lydia Caroline, P. Purushothaman, S. Sevvanthi, G. Vinitha, G. Mani, Growth, spectroscopic studies, and third order non-linear optical analysis of an organic dicarboxylic acid based single crystal: Urea Oxalic acid, Chin. J. Phys. 56 (2018) 1449–1466.
[35] K.K. Irikura, THERMO, PL, National Institute of Standards and Technology, Gaithersburg, MD, 2002.
[36] Leena Sinha, Mehmet Karabacak, V. Narayana, Mehmet Cinar, Onkar Prasad, Molecular structure, electronic properties, NLO, NBO analysis and spectroscopic characterization of Gabapent in with experimental (FT-IR and FT-Raman) techniques and quantum mechanical calculations, Spectrochim. Acta 109 (2013) 298–307.
[37] H. Jacobsen, Localized –orbital locator (LOL) profiles of transition- metal hydride and dihydrogen complexes, Can. J. Chem. 87 (2009) 695–973.
[38] R.G. Parr, W. Yang, Functional Theory of Atoms and Molecules, Oxford University press, New York, 1989.
[39] Ayers, P.W. Parr, R.G. Parr, Variational principals for describing chemical reactions: the Fukui function and chemical hardness revisted, J. Am. Chem. Soc. 122 (2000) 2010–2018.
[40] S. Renuga, M. Karthikesan, S. Muthu, FTIR and Raman spectra, electronic spectra and normal coordinate analysis of N,N-dimethyl-3-phenyl-3-pyridin-2-yl-propan-1-amine by DFT method, Spectrochim. Acta A127 (2014) 439–453.
[41] M. Christophe, G. Andre, T.L. Alejandro, New dual descriptor for chemical reactivity, J. Phys. Chem. 109 (1) (2005) 205–212.
[42] P.K. Chattaraj, B. Maiti, U. Sarkar, Philicity, A unified treatment of chemical reactivity and selectivity, J. Phys. Chem. 107 (2003) 4973–4975.
[43] K. Li, X. Wang, D. Xue, A simple Method for hardness prediction of transition metal compounds, Mater. Focus 1 (2012) 142–148.
[44] A. Dennis Raj, M. Jeeva, R. Purusothaman, G. Venkatesa Prabhu, M. Vimalan, I. Vetha Potheher, 1-((4- methylpiperazin-1-yl)(phenyl)methyl)naphthalene-2-ol;a novel Mannich base organic NLO Crystal for the analysis of electro optic applications, J. Mater. Sci. Mater. Electron. (2017).
[45] R.N. Sheikh, Mohd Anis, M.D. Shirsat, S.S. Hussaini, A Study on optical, dielectric and NLO properties of L-Alanine added ammonium dihydrogen phosphate single crystals, J. Optoelectron. Adv. Mater. 16 (2014) 1147–1152.
[46] U. Von Hundelshausen, Electro Optic effect and dielectric properties of cadmium-mercury-thiocyanate crystals, Phys. Lett. 34A (1971) 7.
[47] S. Stella Mary and S. Shahil Kirupavathy, An insight on spectral, microstructural, electrical and mechanical characterization of Ammonium oxalate monohydrate crystals, Mater. Sci. DOI: .
[48] K.B.R. Varma, K.V. Ramanaiah, K.V. Rao, Linear electrooptic effect in doped KDP crystals, Bull. Mater. Sci. 5 (1983) 39.
[49] Mohd Anis, G.G. Muley, Single crystal growth and enhancing effect of glycine on characteristic properties of bis thiourea zinc acetate crystal, Phys. Scripta 91 (2016) 85801.
[50] A. Vijay, A. Hiremath, Venkatraman, Dielectric, electrical and infrared studies of $\gamma$-$Fe_2O_3$ prepared by combustion method, Bull. Mater. Sci. 26 (2003) 391.